ISSN: 2688-8645

Dynamic Tribological Behavior of a Cone Bit Helical Composite Seal

Yi Zhou, Yi Zhou, Zicong Wang, Yang Jiang

School of Mechatronic Engineering, Southwest Petroleum University, Chengdu, Sichuan 610500, China

Abstract

This study investigated the tribological behavior of helical composite seals for high-speed cone bits under dynamic loading through an integrated experimental–computational approach, systematically elucidating their wear mechanisms. To address limitations of the classical Archard model's static assumptions, an innovative framework for predicting dynamic wear was developed by coupling time-varying contact stress integration with Hertzian contact theory, establishing explicit dynamic correlations among load–geometry wear parameters to enable real-time wear volume prediction. Wear evolution was comprehensively analyzed using a UMT TriboLab tribometer coupled with a three-dimensional white light interferometer for characterizing topography. Cyclic loading spectra were used to quantify wear progression in ball-on-block point contacts with peak loads from 20 to 50 N at frequencies from 1/24 to 1/12 Hz. Experimental results demonstrated an exponential relationship between peak load and wear volume (R^2=0.98), with frequency doubling significantly exacerbating fatigue damage (50.1% greater wear volume at 1/12 Hz than at 1/24 Hz). Stress concentration at helical seal tooth roots formed maximum contact pressure zones, inducing radial propagation of partial-wear cracks. Notably, sealing interfaces maintained effective hydrodynamic barriers even under extreme conditions (400 N or 4 Hz operation). The key findings were verified through synchronous monitoring of the pressure distribution of the interfacial film and transient leakage rates. This study has advanced wear analysis and provided a highly precise theoretical basis for optimizing multiple factors and predicting the service life of the sealing system of deep-drilling equipment.

Keywords

Cone Bit; Helical Composite Seal; Dynamic Loading; Tribological Behavior.

1. Introduction

Roller cone drill bits play a crucial role in deep-well drilling[1- 6]. The bearing seals are vital wearing components that primarily prevent drilling fluid ingress and leakage. The premature failure of these seals is a predominant cause of bearing seizure and catastrophic bit failure, They are also essential in roller cone composite drill bits and roller cone-equipped tools. Current roller cone bit seals operate via passive contact without active sand-flushing capability. During severe bit vibration, sand-laden mud can enter the bearings, causing seal wear. This compromises sealing under varying conditions and accelerates bit failure [7] highlighting a critical need for failure analysis and prevention strategies.

At present, passive contact seals dominate roller cone bit sealing. Traditional O-ring rubber seals are mainstream [8-12]. Recently, section optimization has gained attention, leading to the development of new structures like rectangular, flat, and Y-shaped seals[13-15], there is also shape optimization, such as butterfly seals. [16]. Zhou Shuwen et al.'s asymmetric flat seals show better contact stress distribution via finite element simulation [16]. Subsequently, metal-

ISSN: 2688-8645

sealing technology has emerged. Innovations like bimetallic seals, metal–rubber seals, and single-energizer metal seals (SEMS2) have significantly improved reliability and drilling efficiency compared with O-ring seals[18-21].

Enzhe Bi et al. have conducted in-depth research on the wear of hydrodynamic seals. [22]. Using hydrodynamic theory, Chen et al. designed a new hydrodynamic seal structure, offering a non-contact sealing approach [23,24].

Existing research on wear under dynamic loads mainly focuses on two typical mechanical pairs: the shaft-bearing system and the seal–shaft interface. Regarding shaft-bearing, Priestner and Sun indicated that elastic deformation or bending of the shaft causing metal-to-metal edge contact is a key factor in the performance degradation of sliding bearings. They revealed the intrinsic connection between increased contact pressure, failure of hydrodynamic lubrication, and overestimation of friction loss[25,26]. Fu Jian et al. established a mixed thermal lubrication model for radial shaft seals and were the first to quantify the coupling relationship between the thermal softening of asperities and interfacial wear under high-speed operation [27]. Liu et al. further proposed a method for simulating the multi-scale wear of rotating lip seals. By reconstructing microscopic topography and mapping macroscopic performance, they overcame the limitations of traditional single-scale modeling [28].

In the broader field of wear research, scholars continue to advance classical theories and interdisciplinary integration. Although the classical Archard model established a linear relationship between wear volume, load, and sliding distance, its universality faces challenges in complex operating conditions [29]. Shen X J successfully captured the nonlinear wear evolution under transient loads by applying dynamic contact algorithms to simulate bearing wear[30].Using contact–pressure field reconstruction, Bekesi et al. extended the Archard equation to provide a highly precise tool for calculating reciprocating seal wear depth [31]. Li Chao found that the friction coefficient of vulcanized rubber had a negative correlation with increasing normal load. However, during the wear process, interfacial energy consumption paradoxically increased owing to the enhancement of the stick–slip effect, highlighting the limitations of traditional linear models in wear analysis of flexible materials [32]. Similarly, in the field of fatigue failure analysis, advanced prediction methods integrating energy-based criteria and finite element simulation have been developed to accurately forecast the service life of critical structural connections, showcasing the trend towards physics-based predictive modeling in failure analysis [33] .

To summarize, the failure of roller cone bit seals remains a persistent engineering challenge. most existing roller cone bit seals are passive and lack active sand-flushing function. As a result, they suffer from poor sealing, sand-flushing, and wear, leading to low sealing reliability and ultimately, functional failure. Moreover, there is little research dedicated to the failure analysis on roller cone bit seals under dynamic loads. Therefore, to enhance sealing performance and mitigate failure risks, we designed a spiral-combination sealing structure for roller cone bits. This structure combines spiral seals with O-ring rubber seals and features active sand-flushing capability [7]. This study employs an integrated experimental-computational approach to perform a comprehensive failure analysis. It aims to investigate the wear behavior and characteristics (the failure mechanism) of spiral-combination seals in roller cone bits under dynamic loads, identify the root causes of failure (stress concentration, fatigue damage), and establish a predictive model for failure prevention and service life prediction.

2. Principle of Helical Combination Sealing of a Cone Bit

As shown in **Fig 1**, the spiral-combination sealing structure of a roller cone drill bit consists of a spiral seal and an O-ring rubber seal. It is located in the sealing chamber formed by the roller and bearing. The sealing principle is as follows:

ISSN: 2688-8645

(1) Active sand-flushing: The spiral seal, installed in the spiral groove of the roller's inner hole, rotates with the roller during high-speed drilling. The spiral structure exerts a pumping thrust on the mud. When this thrust balances the external mud pressure, mud entry into the sealing chamber is halted. This pumping action effectively reduces wear from mud particles.

(2) Combination sealing: The O-ring rubber seal is fitted into the bearing groove above the spiral seal. During high-speed drilling, it provides auxiliary two-stage sealing. When drilling stops, the O-ring ensures sealing. This combination meets sealing requirements for different drilling conditions, ensuring high reliability.

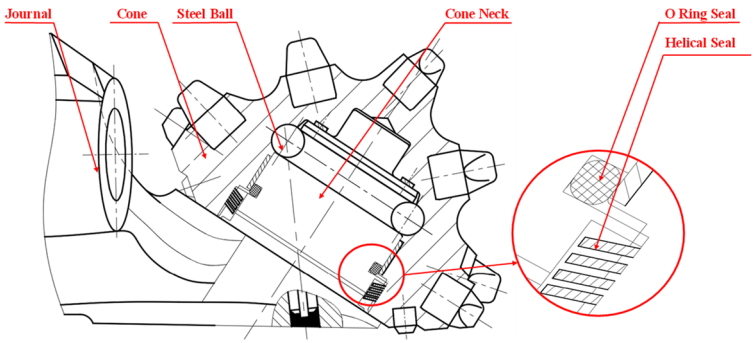

Fig 1. Illustration of the helical composite seal structure of the roller cone bit.

3. Experimental Study

3.1. Test Device

As depicted in **Fig 2**, a UMT TriboLab tribometer was used with a modular dynamic reconfiguration platform with multi-sensing technologies. Equipped with a high-precision force sensor (1 mN–2000 N), the system enables comprehensive tribological characterization across extreme operating conditions (−25 °C to 1000 °C, 5%–99% RH).

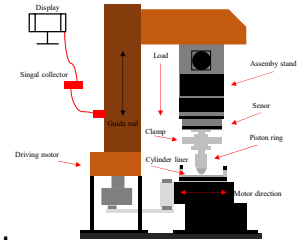

Fig 2. UMT-TriboLab multi-functional tribometer.

3.2. Materials and Specimens

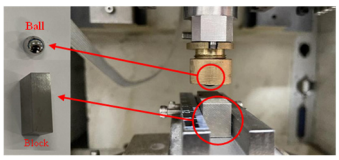

Fig 3. Ball and block specimens

To ensure the experimental accuracy, the experiment was carried out using the point contact of a ball–block model, as shown in **Fig 3**. Because the small width of the teeth of the spiral seal is similar to the size of the point contact with the roller cone bearing, the point contact can more realistically simulate the actual working conditions and reflect the high contact stress. Furthermore, even when the machining accuracy of the test piece is not enough, the point contact can also relatively stably maintain the contact state. This ensures the reliability of the experimental data and makes it easier to quantify the tiny wear.

ISSN: 2688-8645

In the model, the ball, representing the roller bearing, is made of 20CrNiMo[34]. The block, representing the spiral seal, is made of 40Cr. Their physical parameters are listed in Table 1[35,36].

Table 1. Physical properties of material

Material	YieldStrength(σ_s)	Hardness(HR)	ElasticModulus(E)	Poisson'sRatio(ν)	Density (ρ)
20CrNiMo	776 MPa	HRC 60 - 63	208 GPa	0.295	7850 kg/m^3
40Cr	696 MPa	HRC 50 - 55	222GPa	0.3	7700kg/m^3

3.3. Test Scheme

To address the microscale wear characteristics inherent to ball-on-block point contacts, three-dimensional optical microscopy was employed instead of conventional mass loss measurement (with an electronic balance precision of ±0.0001 g) to enhance accuracy. The experimental protocol was as follows.

Post-test block specimens underwent ultrasonic cleaning to remove surface debris. Three-dimensional white light interferometry (3D WLI) with 0.1 nm vertical resolution was used for submicron-level reconstruction of wear scar volume, with volumetric wear rate (mm^3/s) adopted as the quantitative evaluation metric. This approach significantly improved precision and reliability in microscale wear quantification.

The cleaned and dried block specimens were placed on a metallographic microscope stage for surface morphological observation at 100× and 200× magnifications. Systematic comparisons of wear scar topography under varying load enabled identification of dominant wear mechanisms (e.g., abrasion, adhesion) and characterization of surface features (e.g., ploughing grooves, fatigue spalling).

4. Finite Element Model

4.1. Seal Wear Model

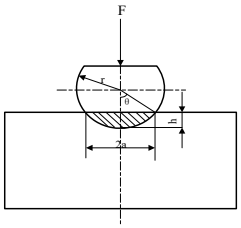

Fig 4. Schematic of the ball-on-block wear contact.

As illustrated in **Fig 4**, the geometric and loading parameters of the ball-on-block contact configuration are defined as follows: r is the ball radius, h is the indentation depth into the block, $2a$ is the contact width, and θ is the contact half-angle, determined by the applied normal load F.

The projected contact area S generated by the ball indenting into the block can be expressed as

$$S = \pi a^2. \tag{1}$$

The normal load in the Dharma model is

$$F = \pi \sigma_5 a^2 \tag{2}$$

ISSN: 2688-8645

The classical Archard wear model exhibits significant limitations under dynamic loading because its quasi-static assumption fails to characterize the nonlinear modulation effects of transient load amplitude/frequency fluctuations on wear behavior. This study presents an improved model [37] tailored for the point-contact characteristics of ball-on-block tribopairs. The proposed model describes the transient effects of periodic loading through integrating the time-varying contact stress $\sigma_0(t)$ and dynamic load function $F(t) = x_0 + 10sin\omega$. By integrating Hertzian contact theory, we establish quantitative relationships among the normal load *F*, contact radius *a*, and wear depth *h.*

The improved model characterizes transient wear behavior through a differential–integral formulation:

$$dh = \frac{k_1 \omega_0(t)}{H_m} dt \tag{3}$$

where K_1 is the dynamic wear coefficient, which incorporates material and working conditions; v is the relative sliding velocity, which is assumed to be constant; $\sigma_0(t)$is the time-varying contact stress, which is associated with the dynamic load via Hertz theory; and $H_m$is the material hardness. The total wear depth is derived as

$$h = \frac{K_1 v}{H_m} \int_0^{t_0} \sigma_0(t) dt. \tag{4}$$

By employing time integration, this formulation captures the accumulation of dynamic load effects, breaking through the static constraints of classical models.

Building on this framework we incorporate Hertzian contact theory to establish a coupled load–geometry–wear relationship, where the normal load and contact parameters are defined as

$$F = \frac{4\sqrt{r}}{3} E^* \sqrt[3]{h^2}, \tag{5}$$

$$a = \sqrt[3]{\frac{3Fr}{4E^*}}, \tag{6}$$

where E^* is the equivalent elastic modulus, and *a* is the contact radius.

The maximum Hertzian contact stress can be formulated as

$$\sigma_0 = \frac{2E^*}{\pi} \sqrt{\frac{h}{r}}. \tag{7}$$

This formulation directly couples wear depth to the local stress field, thereby providing mechanical boundary conditions for calculating dynamic wear. By integrating the above equations, the improved model quantifies transient wear volume. The differential wear volume element is

$$dV_0 = K \left[\theta r^2 l_1 - r^{4/3} l_1 \left(\frac{3F(t)}{4E^*} \right)^{1/3} cos\ \theta \right], \tag{8}$$

where $F(t)$ is the dynamic load function, and θ is the half-angle of penetration. The modified Archard wear volume is derived as

ISSN: 2688-8645

$$V_0 = K\left[\theta r^2 l_1 - r^3 l_1 \left(\frac{3\int_0^{t_S} F(t)dt}{4E^* \int_0^{t_S} dt}\right)^{1/3} cos\ \theta\right]. \quad (9)$$

In this equation, the comprehensive wear coefficient K is

$$K = \frac{V\sigma_S}{v\int_0^{t_0} F(t)dt}, \quad (10)$$

where σ_s is the material yield strength, and v is the cumulative sliding distance.

4.2. Model Establishment

4.2.1. 3D Model Development

Geometric models of the ball (20CrNiMo) and block (40Cr) were created with dimensions consistent with experimental specifications, as illustrated in**Fig 5**. Material properties, including density, elastic modulus, and Poisson ratio (listed in **Table 1**), were defined and assigned to the ball and block. In the assembly module, the ball and block were positioned at their contact interface, with the contact condition specified as hard contact.

4.2.2. Boundary Conditions and Load Application

The block was fully constrained, meaning all degrees of freedom were restricted. The ball retained freedom along the Y and Z axes only, simulating reciprocating motion. Given that each cutting tooth on the roller cone corresponds to a specific region of the helical seal, localized eccentric loading occurs when the teeth engage the formation. This induces contact between the helical seal and roller cone bearing, initiating wear. Because the wear process repeats periodically, the dynamic load was simplified as a normal sinusoidal load applied to the ball. In actual roller cone bit operation, the radial load on the journal reaches approximately 37.74 kN [38]. Based on Hertzian contact theory, the peak dynamic load applied to the tribometer should range between 20 N and 50 N [39].

4.2.3. Mesh Generation

As illustrated Fig 5, a hexahedral mesh (C3D8 elements) was implemented with localized refinement at the ball–block interface. The meshing configuration yielded a total of 71688 elements and 77892 nodes.

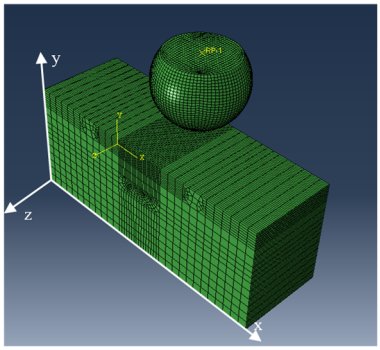

Fig 5. Three-dimensional model, and mesh generation.

4.3. Model Verification

4.3.1. Effect of Peak Dynamic Loads on Wear Behavior

Nonlinear fitting of wear volume under different dynamic load peaks was performed. The fitting coefficient $R^2$was 0.98, indicating that wear volume correlates exponentially with peak load between 20 N and 50 N.

ISSN: 2688-8645

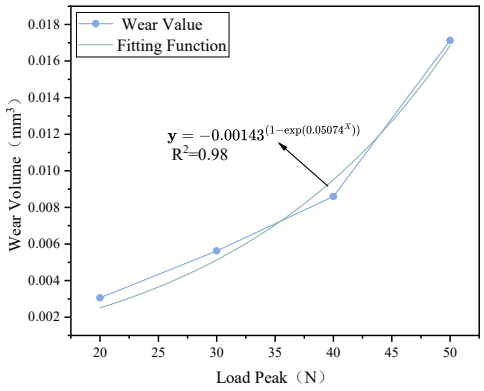

Fig 6. Ball-on-block wear volume as a function of load peak.

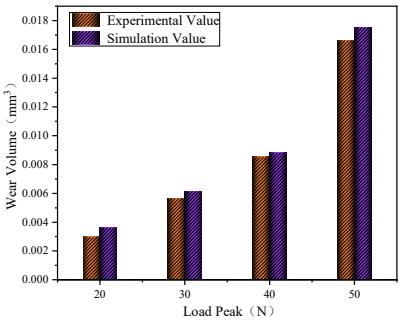

Fig 7. Experimental and simulated wear volumes.

As shown in Fig 6, the experimental data exhibit an exponential trend. Furthermore, the experimental and simulation results closely match under a load of 40 N, as illustrated in Fig 7. The experimental and simulation results only differ by $0.00004mm^3$, demonstrating the wear model's high accuracy and reliability.

Moreover, within the entire loading range (20 - 50 N) when the model was proposed, it also demonstrated relatively high accuracy. The maximum deviation was less than $0.001mm^3$, which confirmed that its robustness was not limited to a single data point.

4.3.2. Effect of Dynamic Loading Frequency on Wear

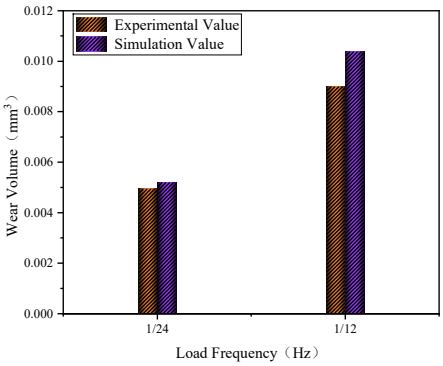

Fig 8. Comparison of experimental and simulated wear volumes under a fixedload with different frequencies.

ISSN: 2688-8645

Under a dynamic loading frequency of 1/12 Hz, the simulated wear volume of the block is 0.01287 mm^3, while the experimental result is 0.01302 mm^3, as shown in Fig 8. The difference between the simulation and experimental results is merely 0.00015 mm^3, demonstrating nearly identical values and confirming the accuracy of the wear model.

When the load peak was fixed at 40 N and the load frequency at 1/24 Hz, the simulated wear volume of the block was 0.00856mm^3. The wear volume at 1/12 Hz was 50.1% greater than at 1/24 Hz. This shows that frequency significantly affects wear under dynamic loading.

4.4. Wear Mechanism Analysis

To elucidate the underlying wear mechanisms, the worn surfaces of the block specimens were examined using metallographic microscopy.

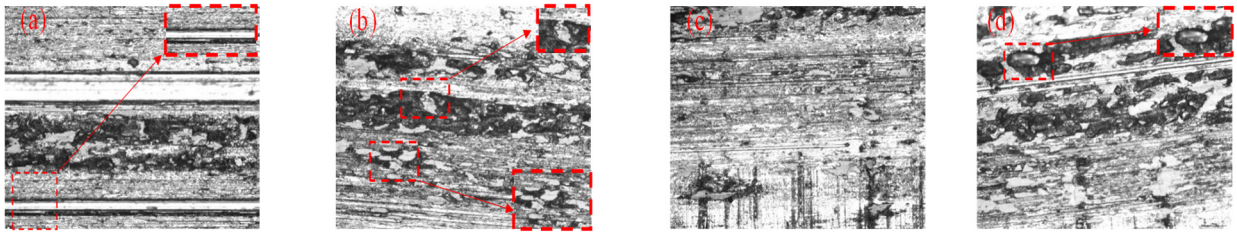

Fig 9. Metallographic wear diagrams under different loads at 1/24 Hz present the wear conditions under the action of loads of (a) 20 N, (b) 30 N, (c) 40 N and (d) 50N.

As show in Fig 9 the evolution of wear mechanisms can be described as follows: the process initiated with abrasive wear as surface asperities were ploughed. Subsequently, the increased contact pressure and temperature promoted adhesive wear. The cyclic nature of the dynamic load inevitably induced fatigue wear, and these mechanisms synergistically accelerated the material removal process, particularly at higher loads and frequencies.

5. Results and Discussion

5.1. Effect of Peak Dynamic Loading on Seal Wear

In actual operating conditions, the load range between the seal ring and cone bearing is 100–330 N. Therefore, dynamic loading peaks of 150–400 N were applied in the simulation. This study investigated the seal wear under peak loads of 150 N, 200 N, 300 N, and 400 N combined with frequencies of 2 Hz, 3 Hz, and 4 Hz. The resulting stress contour plots in Fig 10 reveal the mechanical response under these loading conditions.

As shown in Fig 10, the sealing performance of the helical seal critically depends on the depth of its spiral grooves. According to literature [40] , the optimal groove depth is 2.3 mm, where hydrodynamic effects and leakage flow reach equilibrium, resulting in maximum sealing capacity. Excessive groove depth reduces fluid recirculation efficiency, while insufficient depth fails to establish an effective hydrodynamic barrier, both leading to progressive leakage and eventual seal failure.

However, the line contact between the spiral tooth edges and the bearing induces localized stress concentration (as highlighted in the contour plot), accelerating edge wear and crack propagation. This initiates a vicious cycle of uneven wear: initial wear causes localized groove depths to exceed the optimal value, degrading sealing performance; prolonged wear creates a non-uniform groove depth distribution, with some regions falling below the critical threshold, ultimately leading to hydrodynamic collapse.

As demonstrated in Fig 11, the wear depth remains below 0.4 mm at the maximum loading peak of 400 N. Given that the initial groove depth of the helical seal in this study is 3 mm, computational analysis confirms that even at the 400 N peak load, the effective groove depth (3

ISSN: 2688-8645

mm − 0.4 mm = 2.6 mm) still exceeds the optimal sealing threshold of 2.3 mm. This ensures robust sealing performance. Moreover, the sealing capacity is predicted to gradually improve with progressive wear owing to self-optimization of groove geometry during run-in.

Furthermore, in practical operation where sealing cavity loads are typically below 400 N, extreme vibration-induced uneven wear is confined to localized areas (as marked in Fig 11). Fig 11 shows that the wear depth is less than 0.4 mm when the maximum dynamic load is 400 N. In this study, the groove depth of the spiral sealing ring is 3 mm. Calculation shows that when the maximum peak load is 400 N, the groove depth is still greater than 2.3 mm, which ensures good sealing. As the wear subsequently deepens, the sealing ability will gradually improve. Because the load in the sealing cavity is usually lower than 400 N during the actual process, and the eccentric wear caused by extreme vibration only acts on local areas, it can be concluded that the spiral combined structure can achieve good sealing in actual work. Therefore, the helical composite sealing structure demonstrates reliable sealing under real-world working conditions.

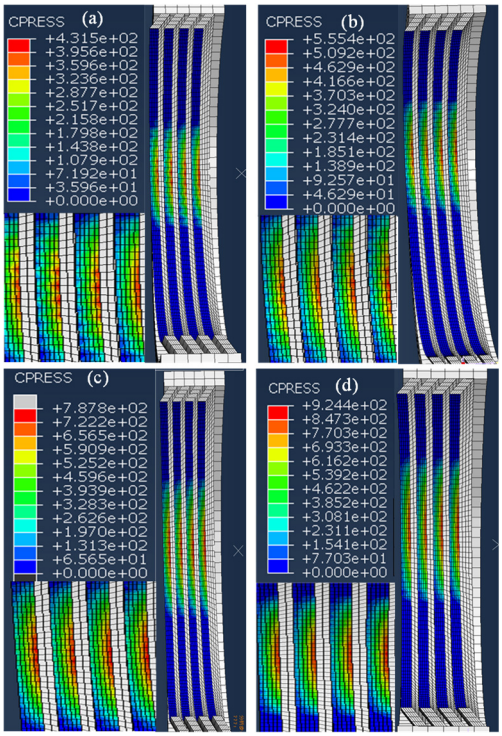

Fig 10. Stress contour plots of the sealing structure under different loads the stress distributions of the helical seal under loads of (a) 150 N, (b) 200 N, (c) 300 N and (d) 400 N are presented.

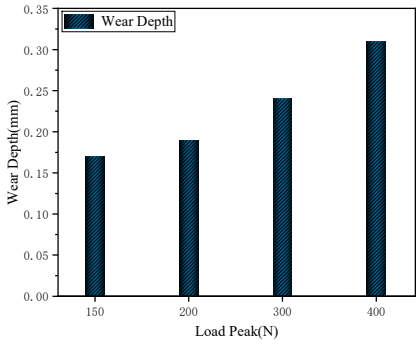

Fig 11. Relationship between peak dynamic loading and wear depth.

ISSN: 2688-8645

5.2. Effect of Dynamic Loading Frequency on Seal Wear

As shown in Fig 12, under a load of 300 N with frequencies of 2 Hz, 3 Hz, and 4 Hz, the maximum contact stress on the threads is also concentrated in the edge regions.

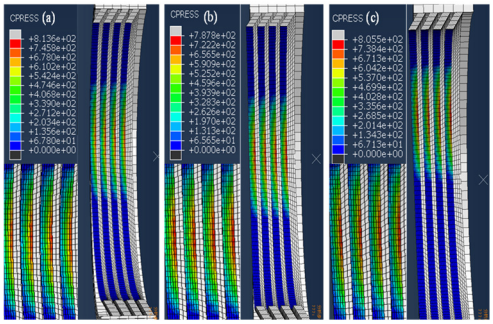

Fig 12. Stress contour plots of the sealing structure under different frequencies the stress distributions of the helical seal under (a) 2 Hz, (b) 3 Hz and (c) 4 Hz are presented.

As evidenced in Fig 13, both experimental and simulation results demonstrate that under identical load amplitudes, high-frequency dynamic loading (4 Hz) exacerbates fatigue wear through increased cyclic counts, leading to a significant rise in wear volume. Taking the 4 Hz/300 N operating condition as an example, the simulation predicts a 0.67 mm wear depth on the seal threads after 40 hours, resulting in a remaining groove depth of 2.33 mm. This value aligns with the theoretically optimal sealing groove depth of 2.34 mm, indicating maintained sealing functionality.

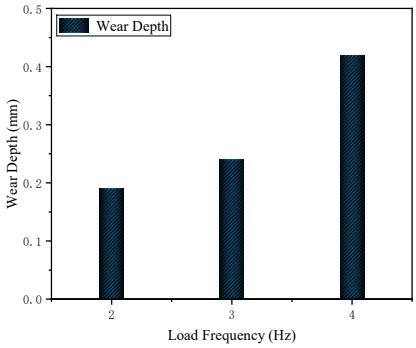

Fig 13. Relationship between dynamic loading frequency and wear depth for the helical seal.

This is attributed to accelerated energy accumulation at the contact interface under high-frequency loading, which promotes fatigue crack initiation and propagation. Furthermore, the synergistic effects of concurrent wear mechanisms—including abrasion, adhesion, and oxidation—collectively increase the material removal rate.

6. Conclusion

This study presents a comprehensive failure analysis of a helical composite seal under dynamic loading, integrating experimental characterization with computational modeling. The key findings and conclusions, which contribute to the prevention of seal failure in roller cone bits, are as follows:

(1) A modified Archard wear model was established that accurately predicts transient contact stresses and wear volumes under various dynamic loading conditions (peak load and frequency). Its high accuracy and robustness were verified through extensive

experimental-simulation comparisons across a wide range of parameters..

(2) The root cause of accelerated wear failure was identified. Wear volume depends exponentially on load magnitude. More significantly, loading frequency exhibits a more profound influence than peak load on wear, directly linking high-frequency dynamics to exacerbated fatigue damage and premature failure.

(3) The failure mechanism was elucidated. Helical seal wear is initiated from the line contact, where the maximum contact stress concentrates at the spiral edges, making these regions the primary failure initiation sites. Under eccentric wear conditions, thread damage progressively extends radially inward, mapping the failure propagation path. Nevertheless, the remaining groove depth under typical loads still maintains effective sealing performance, defining a functional failure threshold.

(4) The proposed seal design demonstrates robust resistance to failure. The helical composite seal exhibits robust performance under parametric variations, maintaining effective sealing at 400 N loads (21% above operational maximum) with <0.4 mm wear depth. It achieves self-optimized groove geometry during run-in, where progressive wear improves sealing efficiency. It tolerates frequency variations up to 4 Hz while retaining hydrodynamic barrier functionality. These findings confirm the design's efficacy in preventing leakage failure under extreme operating conditions.

In summary, this work not only advances the fundamental understanding of the wear-induced failure mechanism in dynamic seals but also provides industry with a practical predictive model and a resilient design solution for enhancing reliability and preventing failure in deep-drilling equipment.

References

[1] Y. Zhou, R. Wang, J. Hu, X. Lei, High-temperature wear mechanism of roller cone bit spiral seal, Wear. 532–533 (2023) 205112.

[2] C. Wang, X. Wang, S. Li, Y. Jiao, R. Yang, G. Li, Evaluation method for tooth wear of roller bits based on the fractal dimension of the rock surface, Journal of Petroleum Science and Engineering. 210 (2022) 110039.

[3] Z. Huang, Q. Li, Y. Zhou, S. Jing, Y. Ma, W. Hu, Y. Fan, Experimental research on the surface strengthening technology of roller cone bit bearing based on the failure analysis, Engineering Failure Analysis. 29 (2013) 12–26.

[4] Y. Zhou,B. Tan, Y. Huang. Sand removal mechanism of a high-speed roller bit with helical sealing, Applied Sciences. 9(18) (2019) 3830.

[5] K. Luo, Y. Ma, K. Meng, J. Jiang, Current research status of metal seals for roller cone bits in oil and gas wells, Lubrication and Sealing. 50(03) (2025) 186–196.

[6] Z. Wu, T. Kou, Y. Cheng, Z. Wang, S. Wang, 2D/3D comparative simulation study on sealing performance of roller cone bit bearing under misalignment, Lubrication Engineering. (2025) 1-8.

[7] Y. Zhou,Y. Tang,Y. Jiang, J. Hu,, X. Huang, Fluid-solid coupling simulation and test of spiral combined seal for high-speed roller cone bit, Acta Petrolei Sinica. 43(4) (2022) 558–565.

[8] X. Jiang, Z. Gan, Research on the Application of O-rings and Dovetail Grooves in Vacuum Sealing, Equipment Manufacturing Technology. (3) (2014) 45-47+55.

[9] J. Wang, X. Gao, Influence of Dimension Tolerance of O-shaped Rubber Sealing Rings on Sealing Performance, Development Innovation of Machinery Electrical Products. (5) (2008) 79-80+95.

[10] W. Wang, S. Zhao, Nonlinear Finite Element Analysis of Rubber O-shaped Sealing Rings, Lubrication Engineering. (4) (2005) 106-107+110.

[11] G. Chen, H. Haiser, W. Haas, Lechner G. Finite Element Mechanical Analysis of O-shaped Sealing Rings, Mechanical Science and Technology for Aerospace Engineering. (5) 2000 740-741+744.

[12] Y. Zhou, T. Li, Y. Zhou, R, Wang. Pressure-Resistant Mechanism of Spiral Magnetorheological Fluid Composite Seal for Roller Cone Bits, Acta Petrolei Sinica. 45(12) (2024) 1851–1862.

[13] T. Liu, L. Tang, Experimental study on sealing-oil storage compensation system for sliding bearings of three-cone roller bits, Oil Field Equipment. (1) (1981) 24–29.

[14] G. Li, Y. Kuang,W. Zhong, Q. Wei, S. Zeng, Research and application of high-temperature-resistant flat rubber seal performance for roller bits, Chinese Petroleum Machinery. 48(8) (2020) 37–42.

[15] B. Chen, Z. Zhang, J. Yang, C. Tan, Y. Jing, X. Luo, Finite element analysis of Y-shaped rubber sealing ring under static sealing conditions, Lubrication Engineering. 34(3) (2009) 72-75.

[16] L. Zhang , X. Wei, A Novel Structure of Rubber Ring for Hydraulic Buffer Seal Based on Numerical Simulation, Appl Sci. 11(5) (2021) 2036.

[17] S. Zhou,Y. Kuang, Q. Wei, Performance study on radial asymmetric flat seal for roller bits, Lubrication Engineering. 48(10) (2023) 60–67.

[18] Y. Zhou, X. Lei, Y. Tang, R.Wang, Z. Yan, W. Bin, Wear study on Ti(C,N)-based cermet seal pair for roller bits, Lubrication Engineering. 49(7) (2024) 96–107.

[19] M. Yu, C. Shen, G. Ma, B. Zhang, L. Shao , C. Gu, W. Nie, Q. Gu, Structural Parameter Optimization of Spring Metal C-shaped Ring Based on Sealing Performance, Lubrication Engineering. 49(7) (2024) 108-114.

[20] H. Yan, Y. Zhao, J. Liu, H. Jiang, Analyses toward factors influencing sealing clearance of a metal rubber seal and derivation of a calculation formula, Chinese Journal of Aeronautics. 29(1) (2016) 292-296.

[21] Y. Ma, Z. Yuan, Y. Ni, X. Meng, X. Peng, Performance prediction and multi-objective optimization of metal seals in roller cone bits, Journal of Petroleum Science and Engineering. 208(Part A) (2022) 109316.

[22] E. Bi, S. Li, A. Liu, K. Chen, Study on the wear characteristics of hydrodynamic seals during start-up based on cross-scale contact mechanics, Wear. 562–563 (2025) 205647.

[23] J. Chen, L. Xu, H. Xu, Fluid dynamic pressure radial seal and its application in petroleum machinery, Chinese Petroleum Machinery. 30(3) (2002) 53–55.

[24] J. Chen, B. Zhang, H. Xu, Research on structure and contact characteristic of Kalsi hydrodynamic seal, Chinese Petroleum Machinery. 33(5) (2005) 15–18.

[25] C. Priestner, H. Allmaier, H. H. Priebsch, C. Forstner, Refined simulation of friction power loss in crank shaft slider bearings considering wear in the mixed lubrication regime, Tribology International. 46(1) (2012) 200–207.

[26] J. Sun , C. Gui, Z. Li, An experimental study of journal bearing lubricationeffected by journal misalignment as a result of shaft deformation underload, Journal of Tribology. 127(4) (2005) 813–819.

[27] J. Fu, B. Hu, H. Ma, T. Yin, Z. Zhang, Y. Fu, Z. Xie. Thermal accumulation effects modelling of radial shaft seal wear and lubrication transition mechanism, Tribology International. 197 (2024) 109747.

[28] D. Liu, S. Wang, C. Zhang. A multiscale wear simulation method for rotary lip seal under mixed lubricating conditions, Tribology International. 121 (2018) 190–203.

[29] J. F. Archard, Contact and rubbing of flat surfaces, Journal of Applied Physics. 24(8) (1953) 981–988.

[30] S. Xue, L. Yun, C. Lei, C. Xiao, Numerical simulation of sliding wear for self-lubricating spherical plain bearings, Journal of Materials Research and Technology. 1(1) (2012) 8–12.

[31] N. Bekesi, K. Varadi, Wear simulation of a reciprocating seal by global remeshing, Periodica Polytechnica Mechanical Engineering. 54(2) (2010) 71–78.

[32] C. Li, H. Huang, J. Qu, J. Cao, F. Huang, Y. Wang, Mechanism of wear and COF variation of vulcanized rubber under changing loads and sliding velocities: interpretation at the atomic scale, Tribology International. 170 (2022) 107505.

[33] C. Mi, W. Liu, C. Wen, Y. Tang, J. Wu, G. Risitano, Fatigue failure analysis and lifetime prediction of self-piercing riveted dissimilar aluminum alloy joint based on energy method, Engineering Failure Analysis. 165 (2024) 108746.

ISSN: 2688-8645

[34] H. Cong, Study on heat treatment and wear resistance of mining roller bit and rolling bearing, Mining Machinery. 37(21) (2009) 11–14.

[35] S. Wu , K. Ma, Mechanical properties test of sliding bearing material for cone bit, Materials for Mechanical Engineering. (11) (2003) 7–9+12.

[36] R. Liang , H. Xiao, W Guan, D. Wang, H. Wang, C. Wang, Analysis on the Causes of Unqualified Mechanical Properties of 40Cr Round Steel, Hebei Metallurgy. (4) (2014) 67-70.

[37] B. Li , J. He, B. Du, H. Xiao, J, Wang. Wear model and finite element analysis of machine tool guide rail based on Archard model, Journal of Mechanical Engineering. 52(15) (2016) 106–113.

[38] R. Wang, L. Zhong, H. Yamg, Y. Chen, Friction and wear properties of roller bit bearing unit specimen, Lubrication Engineering. 38(3) (2013)14–18.

[39] L. Tian, F. Fang, L. Zhu, 133 years of Hertz point contact, Journal of China Three Gorges University (Natural Sciences). 36(2) (2014) 88-97.

[40] L. Li, Study on shaft sealing system of filling pump for drilling pump, Chinese Petroleum Machinery. (4) (1999) 38-41+3.